Chapter 3
Synthesised Structures of *N,N'*-bis(glycinyl)-pyromellitic diimide and its Charge Transfer Complexes

3.1 Introduction

N,N'-bis(glycinyl)-pyromellitic diimide is a functional molecule that rapidly self assembles to form charge transfer (CT) complexes with electron donors (Barooah *et al*., 2003). It is able to do this by being relatively flat as well as containing electron withdrawing groups which are in close proximity to the aromatic ring (Barooah *et al*., 2003). These electron withdrawing carbonyl groups withdraw the electron density associated with the aromatic ring, thereby making that part of the molecule electrophilic. This electrophilic character allows for the attraction of nucleophilic aromatic rings, thereby leading to a vast array of host-guest chemistry options (Kishikawa *et al*., 1999). In this chapter, *N,N'*-bis(glycinyl)-pyromellitic diimide CT structures were synthesised, analysed and compared with those previously published by Barooah *et al*. (2006).

3.2 Experimental

3.2.1 Synthesis of *N,N'*-bis(glycinyl)-pyromellitic diimide (gly-L)

Pyromellitic dianhydride (1.09g, 5mmol) and glycine (0.75g, 10mmol) were added to a 200ml round bottom flask containing boiling stones and 30ml glacial acetic acid. The resulting mixture was allowed to reflux for approximately 10-12 hours at 130°C. The product was then filtered and washed with cold methanol and acetone to remove any remaining starting material, and recrystalised in DMF. The resulting crystals were then washed with cold methanol and a yield of 68% was obtained.

3.2.2 Charge Transfer Complex Formation.

A method was adapted from Barooah *et al*. (2006), in which the 42mg of the *N,N'*-bis(glycinyl)-pyromellitic diimide (gly-L) was dissolved in 7.5ml of methanol. The molar equivalent of the appropriate aromatic compound (naphthalene,

anthracene, phenanthrene and perylene) was then dissolved in 5ml chloroform to form a 1:1 molar complex. The chloroform solution was then layered on to the methanol and allowed to evaporate. All starting materials were obtained from Sigma-Aldrich and were analysed by NMR to check for purity before being utilised.

3.3 Crystal Morphology

3.3.1 gly-L diimide with Various Aromatic Guests

Crystal morphology was studied using an Olympus SZ60 microscope at 30x magnification. From the resulting images it was possible to examine the differences in colour and crystal morphology for all CT complexes obtained.

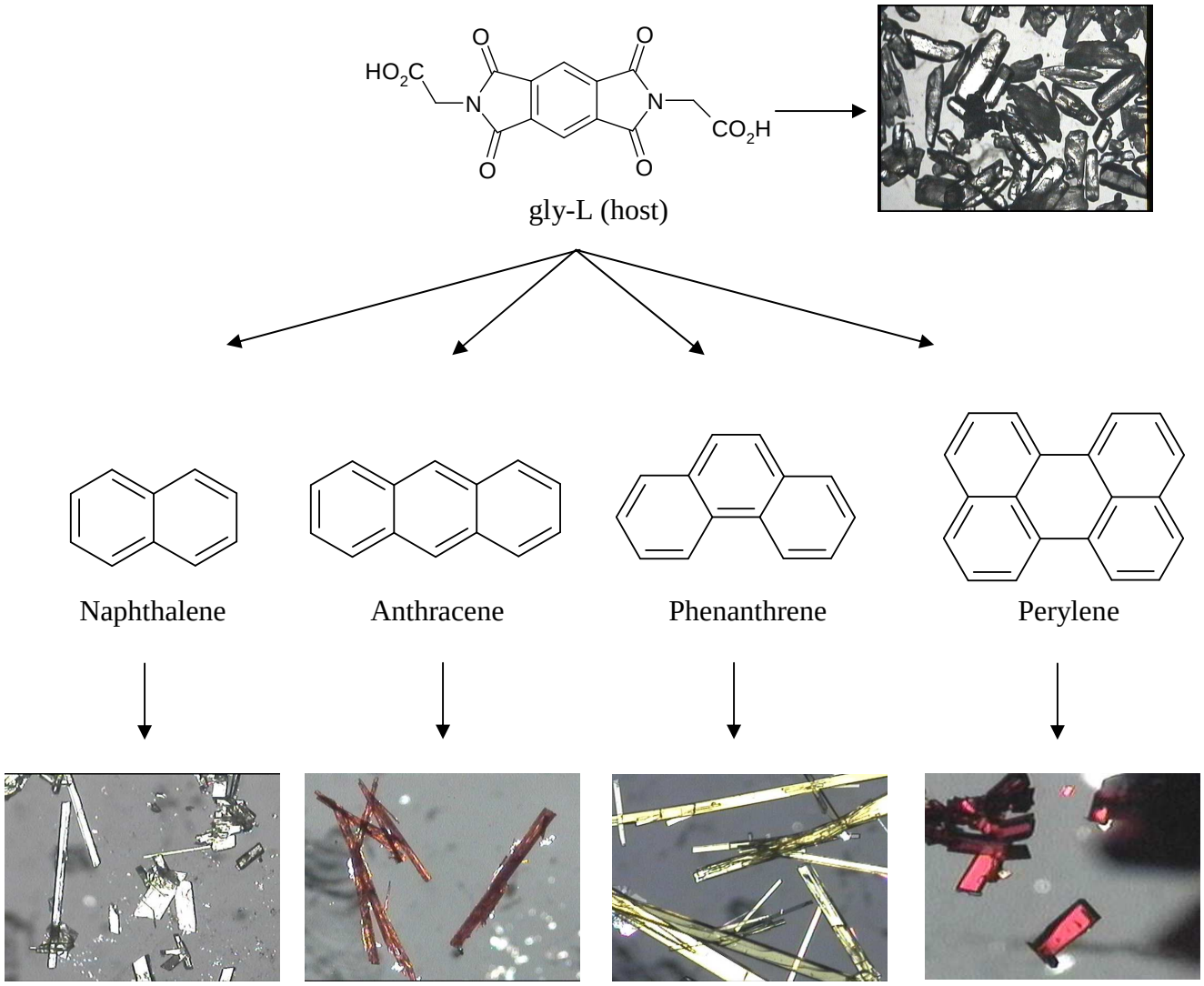

Figure 3.1: Optical microscope images at 30x magnification of gly-L host molecule, with the addition of aromatics donors leading to CT complex formation.

With the exception of the CT complex formed with naphthalene, the crystal structures of anthracene, phenanthrene and perylene have been previously published by Barooah *et al.* (2006). CT complex formation was observed when the starting materials were layered onto each other, and this colour was retained during crystal formation. Crystal morphology showed that the host compound formed colourless prisms whereas all the CT complexes formed coloured needles of various sizes. Yields varied amongst all

complexes from 40 % (gly-NAP), 42% for both (gly-ANT, and gly-PHEN), and 27% for (gly-PERY)

3.4 Single Crystal X-Ray Diffraction

The CT complexes were grown with naphthalene, anthracene, phenanthrene and perylene and analysed by single crystal X-ray diffraction (SCXRD). Attempts to grow CT complexes with benzene, toluene, 4-aminobiphenyl, 4-amino-nitrobenzene, indigo, nitro benzene were unsuccessful.

All CT complexes were examined on a Bruker Apex II diffractometer at -100^{o}C. The crystallographic data of all CT complexes formed with gly-L is shown in Table 3.1 below:

Table 3.1: Crystallographic data for gly-L and CT complexes.

Crystal	**gly-L**	**gly-NAP**	**gly-ANT**	**gly-PHEN**	**gly-PERY**
Chemical formula	$C_{14}H_8N_2O_8$	$C_{24}H_{16}N_2O_8$	$C_{30}H_{26}N_2O_{10}$	$C_{28}H_{18}N_2O_8$	$C_{34}H_{20}N_2O_8$
M_r (g.mol^{-1})	322.22	460.39	574.53	510.44	584.52
Temperature/K	173 (2)	173 (2)	173 (2)	173 (2)	173 (2)
Crystal System	Triclinic	Triclinic	Monoclinic	Triclinic	Triclinic
Space group	*P*-1	*P*-1	$P2_1/c$	*P*-1	*P*-1
a/Å	5.06510 (10)	6.8824 (2)	7.8443 (2)	7.4922 (2)	7.2399 (2)
b/Å	5.1913 (2)	7.6078 (2)	16.6020 (3)	7.7541 (2)	8.8236 (3)
c/Å	12.4280 (3)	10.4753 (2)	10.3328 (2)	20.0138 (4)	10.8033 (3)
α/°	89.053 (2)	79.8160 (10)	90.00	94.0070 (10)	80.271 (2)
β/°	83.091 (2)	70.9010 (10)	106.0160 (10)	99.5480 (10)	77.204 (2)
γ/°	82.593 (2)	83.9360 (10)	90.00	95.2520 (10)	77.724 (2)
V/Å^3	921.707 (16)	509.45 (2)	1293.42 (5)	1137.49 (5)	652.21 (3)
Z, D_{calc}/g cm^{-3}	1, 1.715	1, 1.501	2, 1.475	2, 1.490	1, 1.488
μ/mm^{-1}, F(000)	0.145, 170	0.115, 238	0.112, 600	0.111, 528	0.108, 302
Crystal size/mm	0.39 × 0.28 × 0.03	0.55 × 0.20 × 0.11	0.59 × 0.12 × 0.10	0.38 × 0.11 × 0.08	0.57 × 0.09 × 0.4
Absorption correction	None	None	None	None	None
θ_{max}/°	34.61	28.27	29.96	28.30	28.41
h, *k*, *l* (min, max)	(-8, 8), (-8, 8), (-19, 18)	(-9, 9), (-10, 10), (-13, 13)	(-11, 11), (-21, 23), (-13, 14)	(-9, 9), (-9, 10), (-26, 26)	(-9, 9), (-11, 11), (-14, 14)
Reflections collected	11551	8270	15791	29418	10430
Unique reflections	2691	2513	3740	5610	3283
Observed reflections	1328	2050	2467	3017	2113
No. of parameters	109	155	198	343	199
R_{int}	0.0667	0.0489	0.0533	0.0785	0.0710
R_1 , wR_2	0.0495, 0.0968	0.0384, 0.0987	0.0492, 0.1113	0.0429, 0.0857	0.0432, 0.094
R_1, wR_2 (all data)	0.1252, 0.1141	0.0481, 0.1040	0.0775, 0.1217	0.0968, 0.1120	0.0753, 0.1046
GoF	0.897	1.055	1.025	0.908	0.917
$\Delta\rho_{max}$, $\Delta\rho_{min}$ (e Å^{-3})	0.285, –0.349	0.300, –0.243	0.270, –0.357	0.268, -230	0.223, -0.233

Table 3.1 indicates that all structures except for gly-ANT crystallised out in a centrosymmetric space group (*P*-1), with a triclinic crystal system. This commonality amongst structures indicates similar packing arrangements of molecules within the unit cell. The host molecule structure (gly-L) contained the highest crystal density.

Comparing these structures obtained through SCXRD, allowed us to further compare and contrast the molecular interactions amongst all CT complexes, as discussed below.

3.5 Structural Analysis

3.5.1 *N,N'*-bis(glycinyl)-pyromellitic diimide (gly-L)

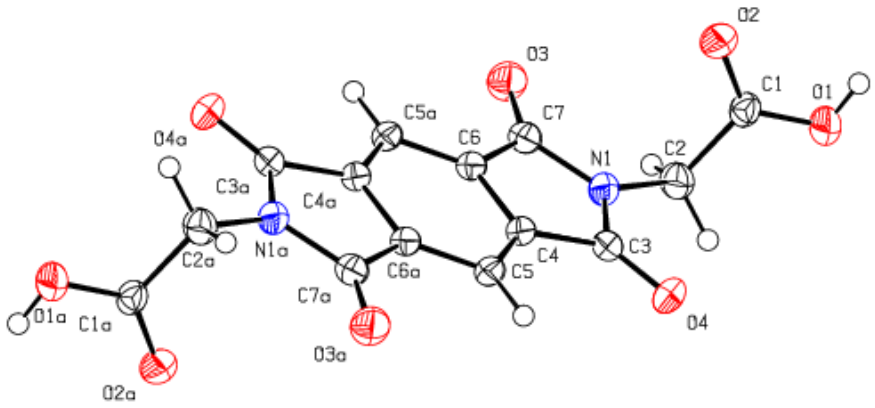

Figure 3.2: Ortep diagram for gly-L drawn at the 50% probability level.

gly-L crystallises as colourless prisms in a triclinic, *P*-1 system. The asymmetric unit contains half the molecule, which occupies a centre of inversion. With the exception of the carboxylic acid groups, the molecule is relatively planar as indicated in the figure 3.2. This planarity coupled with polar carbonyl groups and π acceptor sites are crucial for the formation of host guest complexes with suitable donor aromatic compounds. A key feature of this molecule is the *trans* arrangement of the carboxylic acid groups, which occurs at an angle of 112.08^{o} with respect to the aromatic plane. The consequence of this geometry is the formation of a step like arrangement of

molecules through moderate inter-molecular hydrogen bonding, as outlined in figure 3.3.

3.5.1.1 Hydrogen Bonding

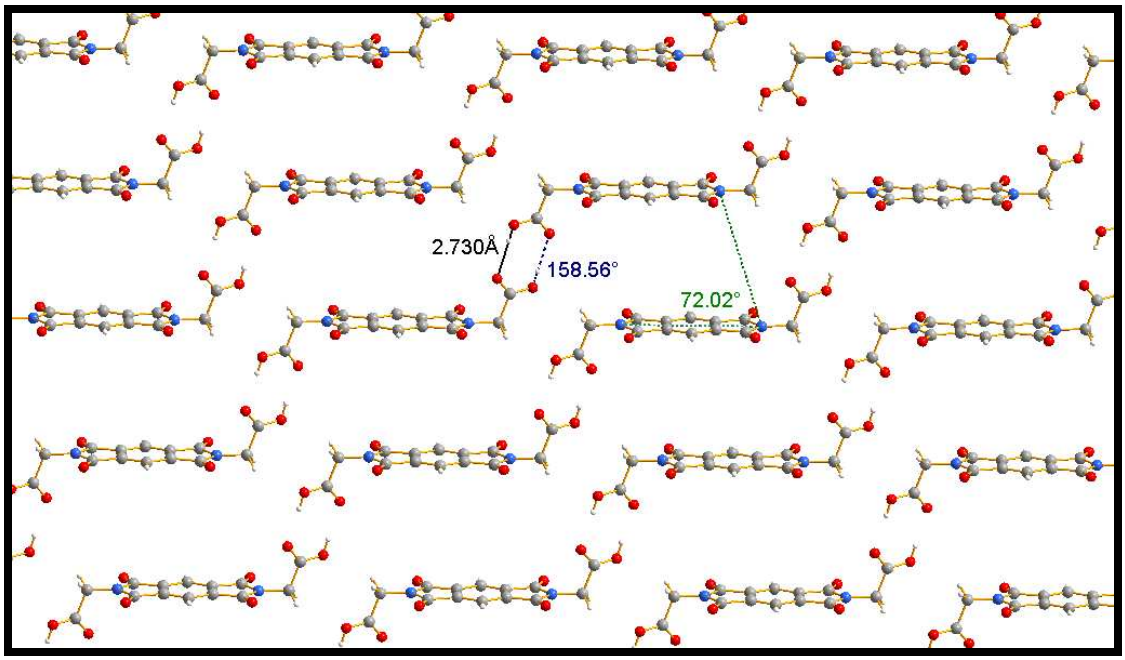

Figure 3.3: Two dimensional layer of gly-L molecules interacting through hydrogen bonding between carboxylic acids.

The above figure illustrates a two dimensional extension of the crystal structure of gly-L. This molecule self assembles through inter-molecular hydrogen bonding between the carboxylic acid groups through O1—H···O2 (d $_{O1\cdots O2}$ 2.730Å; ∟D—H···A 158.56°) which leads to a hydrogen bonded ring defined by the $R^2_2(8)$ graph set. Crystal packing indicated the presence of stacked/layered structure in which the H-bonded ribbons of molecules do not directly overlap over each other. Instead they form an offset 2D stacking arrangement with an angle of 72.02^o (N1-N1-N1) coupled with an inter-planar distance of 3.27Å between adjacent 2D layers. According to Barooah *et al*. (2006) the offset stacking arrangement happens to maximise the dipolar interactions between the π electrons and the hydrogen atoms on the diimide unit.

Space filling representation of the 2D stacks results in the formation of small voids, thus permitting the incorporation of a donor molecule in charge complex structures, figure 3.4.

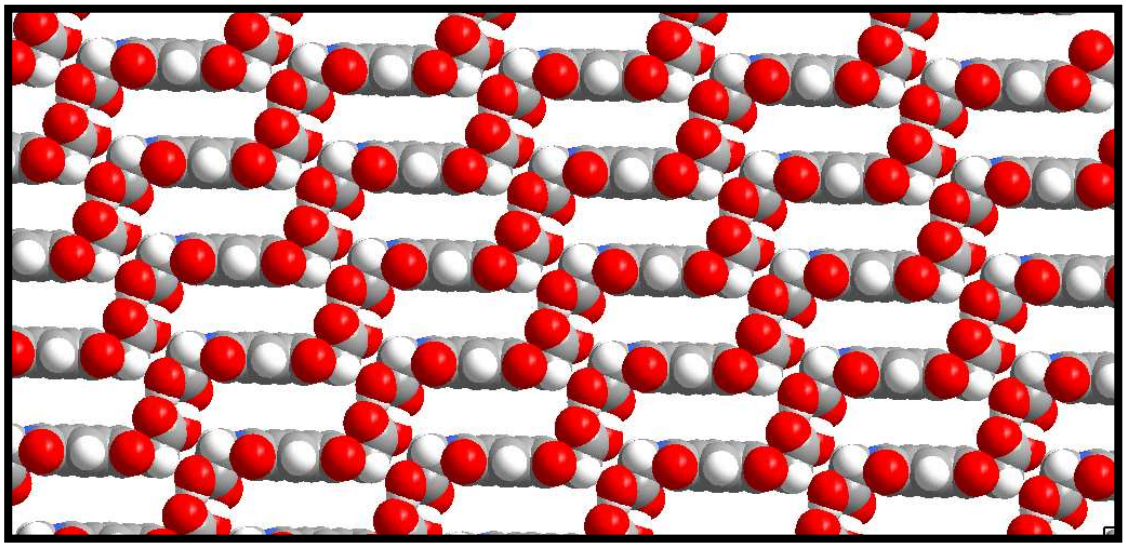

Figure 3.4: Space fill diagram of a 2D layer, indicating the presence of voids in the structure of gly-L.

3.5.2 Charge Transfer Complexes

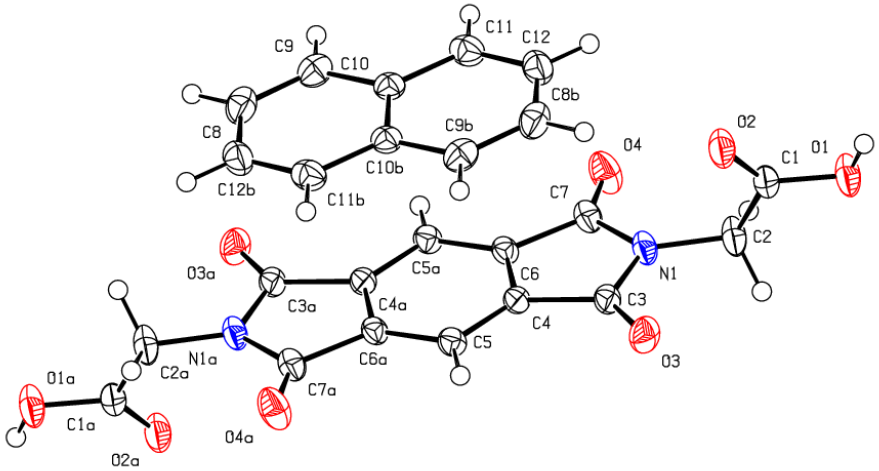

gly-NAP

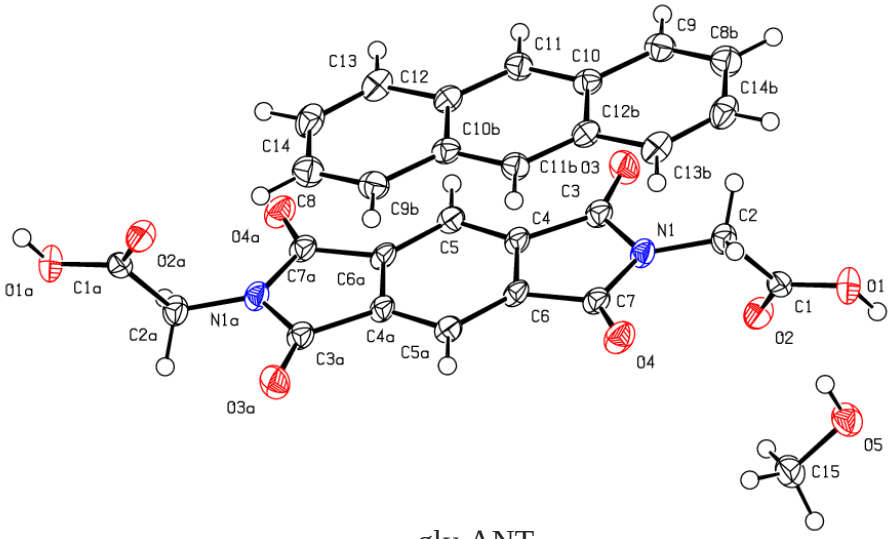

gly-ANT

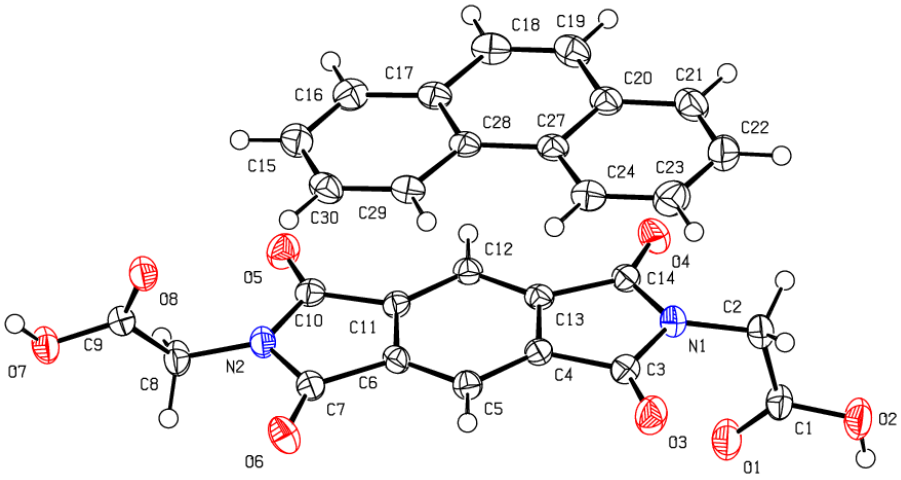

gly-PHEN

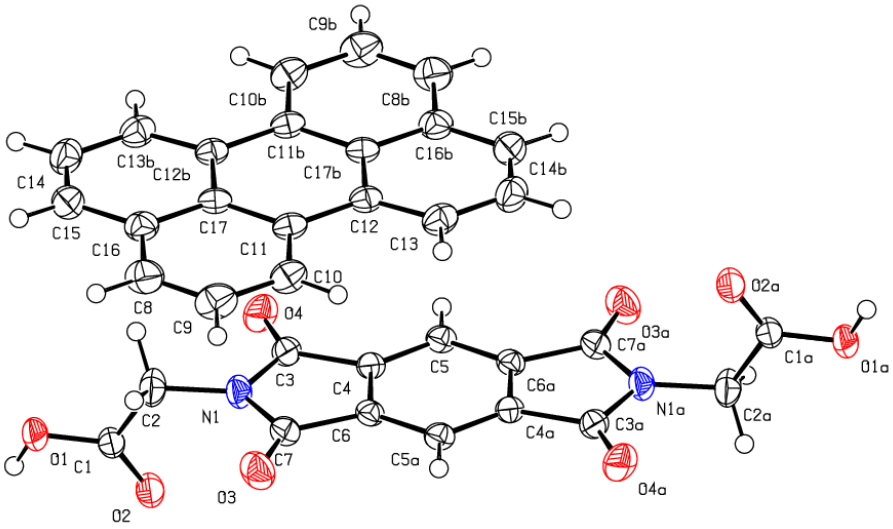

gly-PERY

Figure 3.5: Ortep diagrams of CT complexes drawn at the 50% probability level.

CT complex crystals vary in colour due to electronic charge being transferred from a donor to an acceptor molecule. The difference in electronic charge depends on the strength of the interaction between the donor and acceptor, and is directly linked to the size, shape and conjugation of the aromatic donor. Colours varied from light yellow (gly-NAP), to yellow (gly-PHEN), to orange (gly-ANT) and lastly to red (gly-

PERY). Of all the CT complexes formed with gly-L, only gly-ANT contained a methanol solvent molecule within its unit cell, whereas gly-PHEN was disordered across two positions. All the CT complexes were centrosymmetric, with additional symmetry elements for gly-ANT in the form of a glide plane and a two-fold rotation axis. All the aromatic compounds used formed a 1:1 molecular complex with gly-L.

The formation of the CT complexes leads to the adjustment of the terminal *trans* carboxylic acid geometry (N1–C2–C1) of the host molecule. Angles deviated from the original 112.08^{o} to 112.55^{o} (gly-NAP), 115.12^{o} (gly-ANT), 114.88^{o} and 110.22^{o} (gly-PHEN) and 114.54^{o} (gly-PERY). This difference is due to the accommodation of the donor and solvent molecules. Each carboxylic acid group within the complexes contained the same angle of rotation, except for gly-PHEN due to distortion of the host.

3.5.2.1 Hydrogen Bonding of CT Complexes

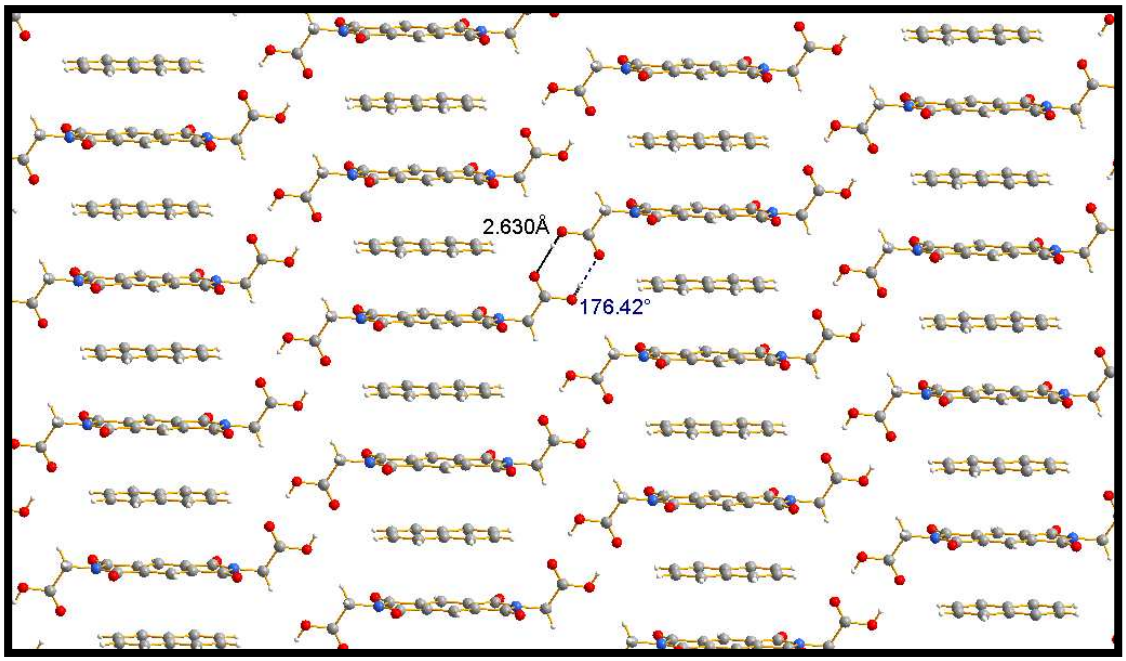

gly-NAP

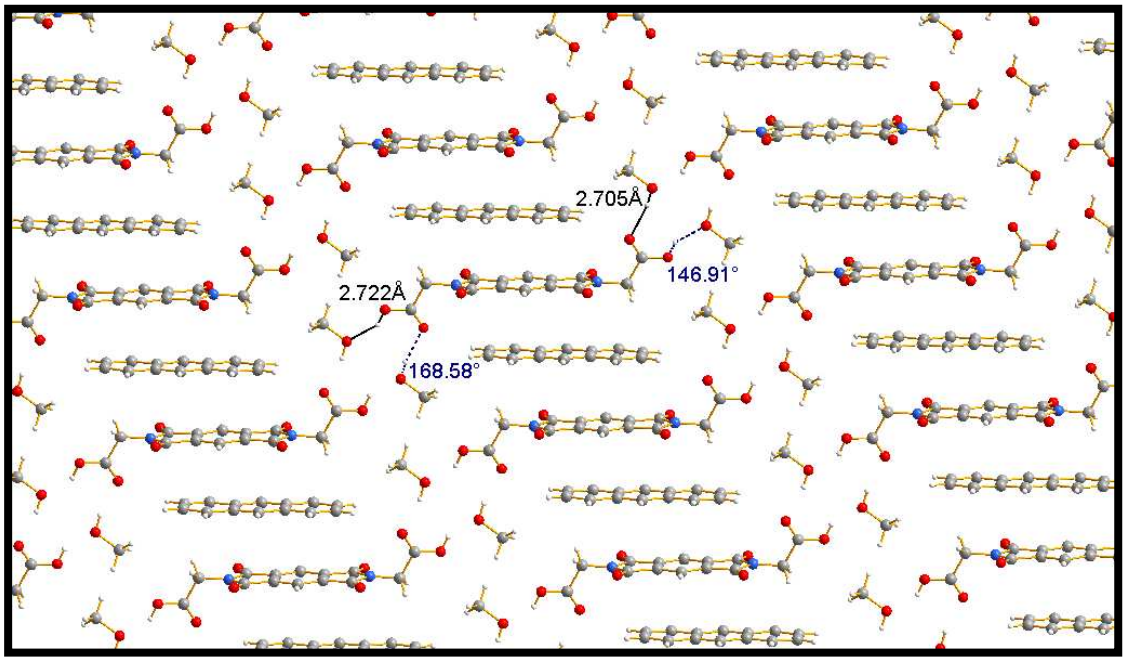

gly-ANT

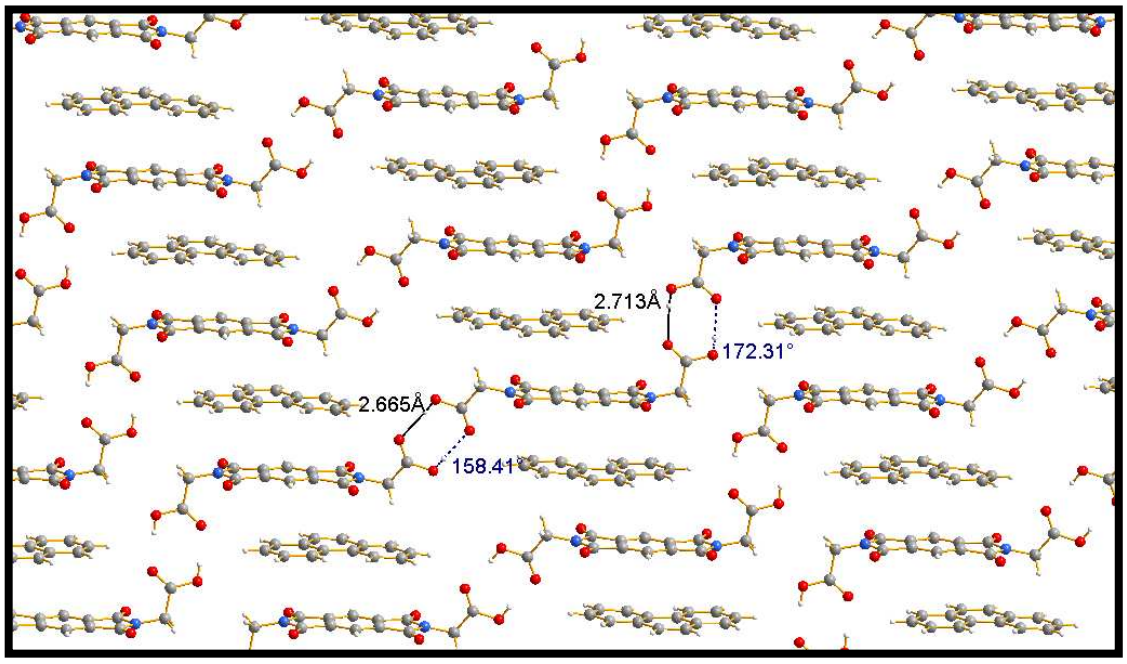

gly-PHEN

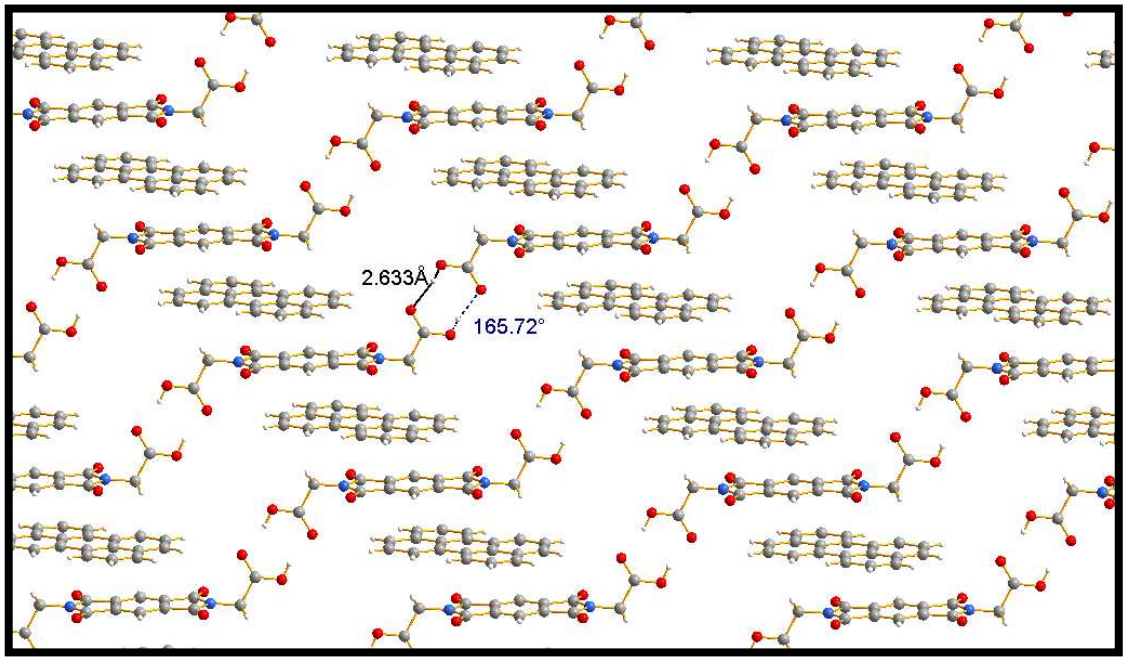

gly-PERY

Figure 3.6: Two dimension layer formation through CT interactions and H-bonding.

Moderate inter-molecular hydrogen bonding between the carboxylic acid groups allows each CT complex to extend infinitely in two dimensions with a step-like arrangement, as indicated in figure 3.6. The bond lengths and angles associated with each CT extension is given in table 3.2. A R^2_2 (8) hydrogen bonding ring pattern was observed for gly-NAP, gly-ANT and gly-PERY, whereas a R^4_4 (12) pattern was adopted for gly-ANT. The difference in bonding patterns is attributed to the incorporation of the methanol molecules between the carboxylic bridges. All CT complexes exhibit symmetrical packing of aromatic compounds, except for gly-PHEN which contains alternate stacking arrangements of the phenanthrene molecule, due to its shape. The accommodation of the donor molecules also leads to a change in the 2D offset stacking arrangement of the host molecules. The offset stacking angles changed from 72.02^o (gly-L) to 85.40^o (gly-NAP), 63.70^o (gly-ANT), 63.98^o (gly-PHEN) and 56.62^o (gly-PERY). This illustrates that an increase in aromatic size decreases the 2D offset stacking angle.

Table 3.2: Intermolecular hydrogen bonding between gly-L molecules in the CT complexes studied.

CT complex	Interaction	D—H/Å	H···A/Å	D···A/Å	∟D—H···A/°
gly-NAP	O1—H···O2	0.840	1.790	2.629(2)	176.42(7)
gly-ANT	O1—H···O5	0.840	1.882	2.626(2)	146.93(8)
gly-ANT	O5—H···O2	0.840	1.865	2.694(2)	168.89(9)
gly-PHEN	O2—H···O1	0.840	1.873	2.707(2)	172.36(10)
gly-PHEN	O7—H···O8	0.839	1.826	2.625(2)	158.49(9)
gly-PERY	O1—H···O2	0.840	1.793	2.615(2)	165.72(8)

Both gly-NAP and gly-PERY carboxylate bridges are equidistant, whereas the gly-ANT and gly-PHEN are not. This is due to the incorporation of the solvent methanol molecules for gly-ANT and the alternate stacking arrangements of the phenanthrene molecules found in gly-PHEN.

All CT complexes are further stabilised by weak interactions, such as CH···O, CH···π and π···π interactions, between the host molecules (gly-L–gly-L) and the host guest molecules (gly-L–aromatic). These interactions enable the structure to extend infinitely into in the second and third dimension (2D and 3D) (figure 3.7 and table 3.3).

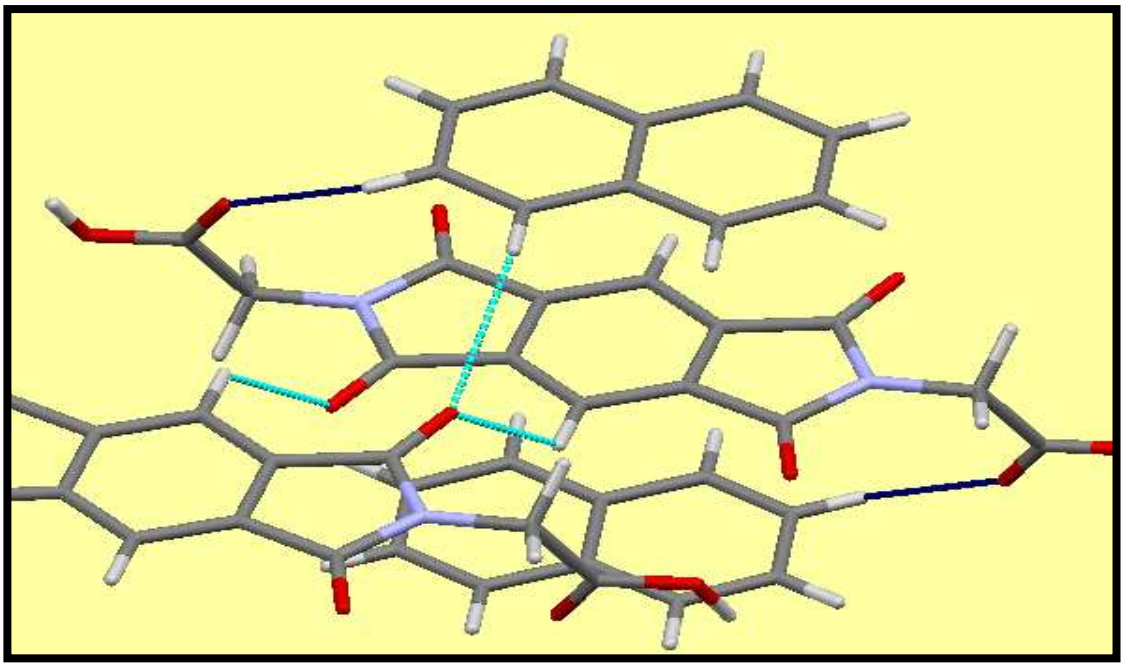

Figure 3.7: Weak (C-H···O) intermolecular hydrogen bonding amongst terminal (navy bonds, 2D) and planar carbonyl groups (turquoise, 3D) in gly-NAP.

Two dimensional stacking occurs mainly through CH···O interactions amongst the terminal carbonyl and the aromatic donor molecules. The 2D stacks of gly-PHEN and gly-PERY are further stabilised by CH···π and CO···π interactions. [C8—H8a···*Cg*: d $_{C\cdots\pi}$ 3.269Å; ∟D—H···A 132.00° and C10—O5···*Cg*: $_{C\cdots\pi}$ 3.523Å; ∟D—H···A 60.90° (gly-PHEN) and C2—H2a···*Cg:* d $_{C\cdots\pi}$ 3.607Å; ∟D—H···A 141.00°; C7—O3···*Cg*: d $_{C\cdots\pi}$ 3.611Å; ∟D—H···A 72.35° and C3—O4···*Cg*: $_{C\cdots\pi}$ 3.450Å; ∟D—H···A 72.64° (gly-PERY)].

Table 3.3: CH···O interactions stabilising layers in the various CT structures.

CT complex	Interaction	D—H/Å	H···A/Å	D···A/Å	∟D—H···A/°
gly-NAP	C8—H···O2	0.950	2.594	3.554(9)	117.91(9)
gly-ANT	C8—H···O2	0.950	2.690	3.641(3)	128.22(10)
gly-PHEN	C22—H···O1	0.951	2.661	3.612(3)	135.02(10)

Table 3.4: List of weak gly-L–gly-L (g-g) and aromatic–gly-L (a-g) CH···O interactions stabilising the CT complexes studied.

CT complex	Interaction	D—H/Å	H···A/Å	D···A/Å	∟D—H···A/°
gly-NAP (g-g)	C5—H···O3	0.950	2.540	3.490(2)	130.13(8)
gly-NAP (a-g)	C9—H···O3	0.950	2.514	3.464(10)	134.09(8)
gly-ANT(g-g)	C2—H_B···O4	0.990	2.515	3.505(3)	128.89(9)
gly-ANT (a-g)	C14—H···O3	0.950	2.697	3.647(2)	172.07(10)
gly-PHEN (g-g)	C2—H_A···O3	0.991	2.696	3.687(3)	159.80(10)
gly-PHEN (a-g)	C19—H···O6	0.950	2.562	3.512(3)	149.30(10)
gly-PHEN (a-g)	C29—H···O4	0.950	2.461	3.411(3)	131.09(10)
gly-PERY (a-g)	C10—H···O4	0.950	2.678	3.628(3)	173.37(10)
gly-PERY (a-g)	C13—H···O4	0.951	2.479	3.430(2)	162.40(10)

CT structures extend to form step-like arrangements through moderate intermolecular hydrogen bonding and charge transfer related interactions within the 2D stacking arrangements. With the exception of gly-ANT, all 2D stacked sheets amongst the CT complexes align up in a parallel fashion resulting in the extension of the structure into the third dimension. This configuration adopted by the CT complexes is due to the formation of CH···O interactions between the 2D parallel sheets, which is due to host-host and host guest interactions. gly-ANT adopts a zigzag conformation between the adjacent stacked sheets of the complex due to the CH···O interactions between the methanol molecules of the one layer with the diimide carbonyls of another. The methanol molecules incorporate within the carboxyl bridges of gly-ANT and serves to further stabilise the framework through weak intermolecular hydrogen bonding C5—H···O5 ($d_{C5\cdots O5}$ 3.544Å; ∟D—H···A 169.00°).

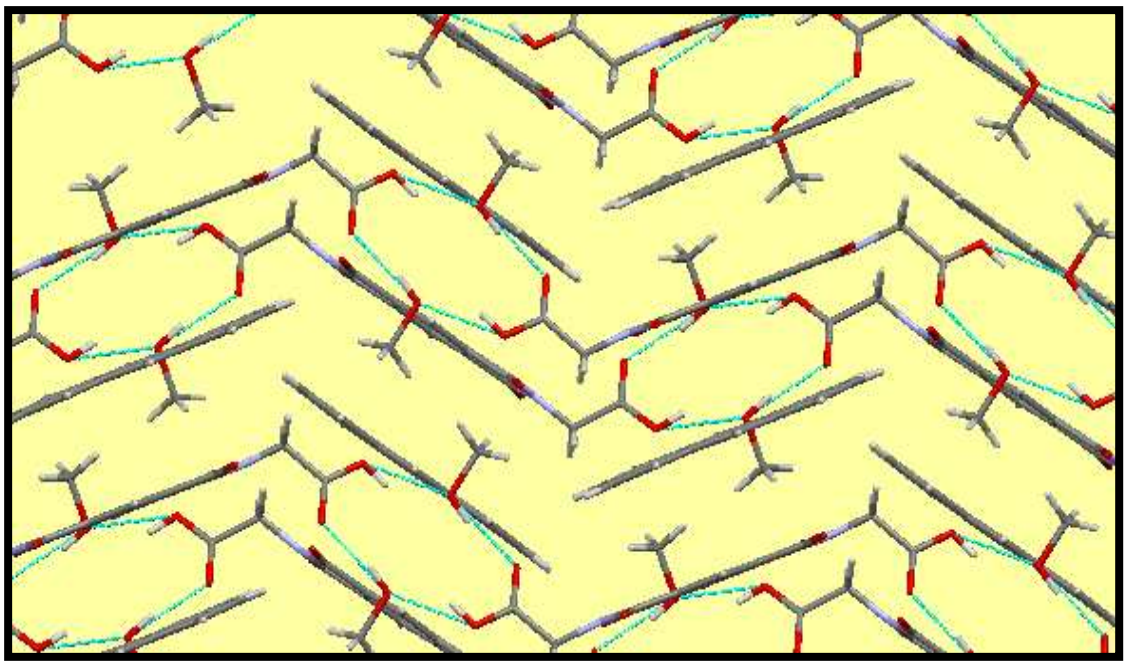

Figure 3.8: Three dimensional extension of gly-ANT indicating zigzag arrangement between adjacent sheets.

All CT complexes formed π···π interactions which where responsible for the stability and stacking arrangement found within each structure. Interplanar π···π distances between the aromatic donor and the host molecules (acceptor) varied amongst the CT complexes, with gly-NAP having a closest *Cg*···*Cg* interplanar distance of 3.40Å, gly-ANT (3.50Å), gly-PHEN (3.31Å and 3.56Å) and gly-PERY (3.37Å). Only gly-PHEN contained two different distances between the host and the aromatic donor, and this was due to the alternate stacking arrangements of the phenanthrene molecules. All π···π interactions found within the CT complexes were within the normal range of 3.6Å as defined by Hunter and co-workers (1990).

3.6 Lattice Energy Calculations

Lattice energy calculations were performed using the Oprop module of the OPiX program (Gavezzotti, 2003). These calculated energies correspond to the molecule-molecule interactions and was used to identify which molecular geometries contribute most to the overall lattice stabilisation. From the calculations performed on the gly-L

host and CT complexes, total lattice energies of -688.90kJ/mol were calculated for gly-ANT, -628.80kJ/mol for gly-PERY, -563.60kJ/mol for gly-PHEN, -517.40kJ/mol for gly-NAP and -444.80kJ/mol for gly-L. All CT complexes revealed three similar molecular arrangements that make the most significant contribution the total lattice energy of the structures. These molecular arrangements coincided with CT π···π interactions (I), OH···O interaction between the carboxylic bridges (II), and aromatic hydrogen (ArH) bonding to planar diimide carbonyl (IC) (III). The arrangement of these molecules with respect to the host molecule (black) is illustrated below using gly-NAP as an example (figure 3.9) along with their respective energies (table 3.5).

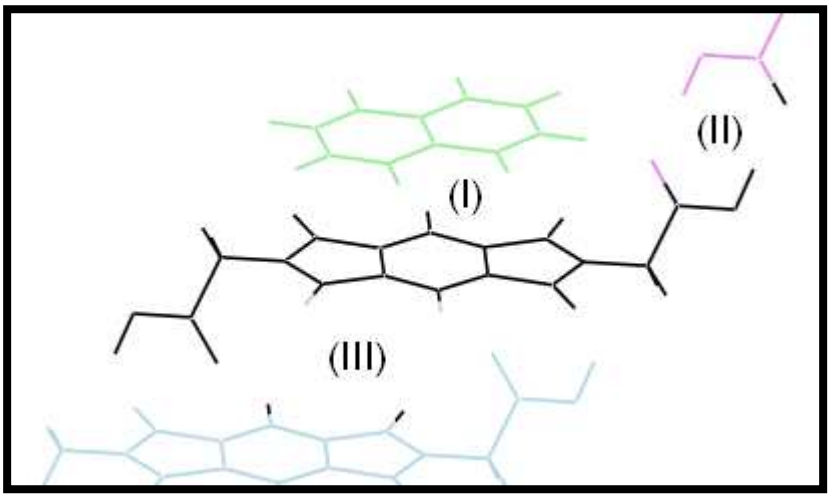

Figure 3.9: Structural arrangement of molecules for gly-L CT complexes contributing most to the stability of the structure.

Table 3.5: Energy values (kJ.mol^{-1}) associated with common molecular conformations adopted by all structures using gly-L.

Structure		gly-L	gly-NAP	gly-ANT	gly-PHEN	gly-PERY
Interaction						
(I)	π···π		-53.4	-65.8	-65.2 & -61.7	-72.0
(II)	O-H···O	-49.7	-48.0	-25.6 & -21.0	-49.3 & -42.4	-47.5
(III)	Ar-H···O		-26.0	-10.0	-13.7 & -11.9	-32.3

Table 3.5 indicates that gly-PHEN contains two values for interactions (I)-(III). This is due to the phenanthrene molecule being disordered over two positions due to the asymmetric shape of the molecule with each value representing one of these orientations. Besides the energies associated with the molecular interactions above, there are arrangements that were unique to individual structures. These included 3D offset stacking of the host molecule found in the gly-L structures associated with energy contributions of -61.3kJ/mol and -44.4kJ/mol for gly-L (figure A1.1). The host molecule associated with gly-L and gly-PERY structures adopted the same molecular arrangement with stabilising energies of -20.1kJ/mol (gly-L) and -14.2kJ/mol (gly-PERY). This energy is corresponded to a CH···O interaction between the alkyl and terminal glycinyl carbonyl (GC) group within the 3D layers.

The three other CT complexes (gly-NAP, gly-ANT and gly-PHEN) each had an energy contribution of -13.8kJ/mol, -17.8kJ/mol, -11.6kJ/mol. This stabilising energy corresponds to the molecular arrangement coinciding with a CH···O interaction, from the alkyl group to the planar IC carbonyl, within the 3D structure. Of all the structures only gly-ANT has a molecular orientation within the 3D structure in which ArH interacts with the GC carbonyl. This orientation resulted in a stabilising energy of -31.7kJ/mol, and is due to the presence of the methanol molecules within the structure.

The tabulated (table 3.5) data obtained from the lattice energy calculations indicated that the most significant stabilising energies for the CT complexes were due to π···π

interactions, and 3D offset stacking of the host molecule (gly-L).From the above table and the obtained lattice energy calculation, it was noted that the most significant stabilising energies for the CT complexes were due to π···π interactions, and 3D offset stacking of the host molecule (gly-L). The next most important contributions to lattice energy were the OH···O carboxylic bridges. The molecular arrangements of the third, fourth and fifth most stabilising interactions varied amongst all structures. Interactions included CH···O interactions between the alkyl and aromatic hydrogen groups with the IC and GC carbonyl groups, to the weak OH···O interaction. (See appendix for full molecule-molecule interactions).

3.7 PXRD Data

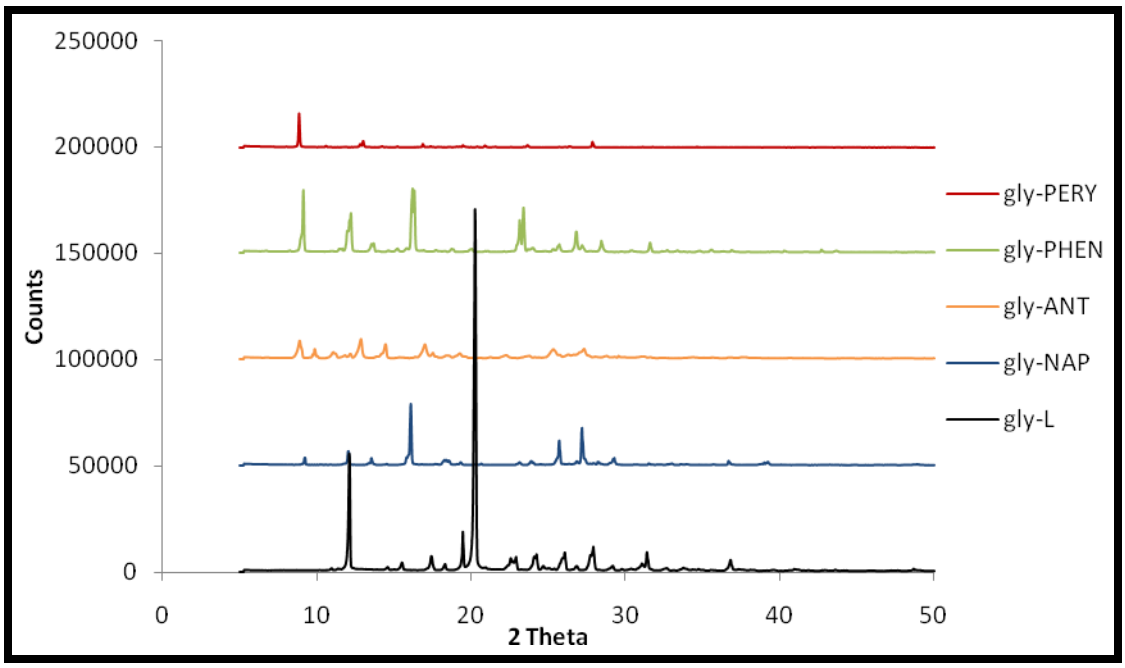

Figure 3.10: Experimental X-ray powder diffraction pattern of gly-L and CT complexes.

All PXRD data was obtained by grinding samples in air and placing them in a Bruker D2 Phaser diffractometer. Figure 3.10 illustrates the various observed PXRD pattern for structures. The observed PXRD patterns for gly-L and gly-ANT did not correlate well with the calculated powder patterns. A reason for this deviation in the gly-ANT

pattern could be due to solvent evaporation of methanol upon grinding, and the presence of an impurity in the form of starting material for gly-L. The other CT complex experimental powder patterns were found to match the calculated powder patterns using their respective single crystal data, as outlined in the appendix.

3.8 Thermal Analysis

3.8.1) Thermogravimetric Analysis (TGA)

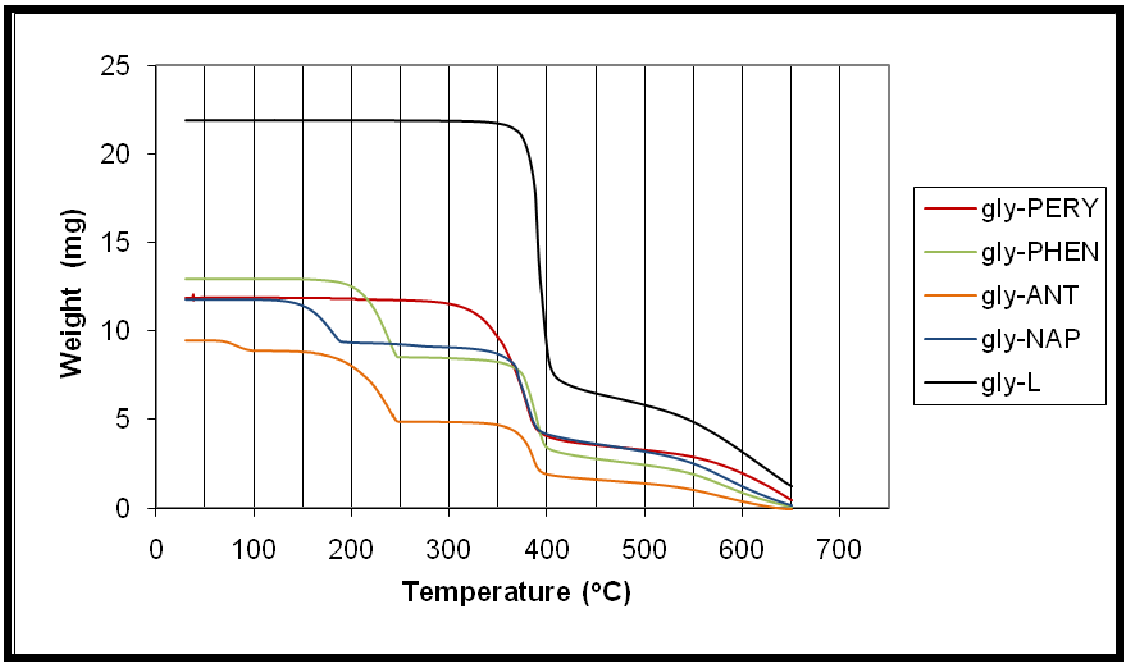

Figure 3.11: Thermogravimetric trace for gly-L and CT complexes.

The TGA analysis of the CT complexes all showed variable step formations, ranging from two to four steps. The above figure 3.11 indicates a two step decomposition of gly-L. This material is thermally stable up to temperatures of 357^{o}C, which was then followed by a weight loss of 78.6% (17.25mg) for the first step, followed by an additional loss of 17.1% (3.76mg) after 537^{o}C. It was noted that all CT complexes followed the same degradation pattern of gly-L at temperatures higher than 350^{o}C. Thermal stability of the CT complexes varied from 140^{o}C for gly-NAP, 165^{o}C for gly-PHEN and 284^{o}C for gly-PERY. Loss of the donor in each of these CT complexes leads to a weight loss of 20.8% (2.46mg), 34% (4.41mg) and 25%

(2.96mg) respectively. gly-ANT contained methanol solvent molecules that were liberated below 100^{o}C, and resulted in a weight loss of 5.6% (0.53mg) followed by an additional 44.5% (4.21mg) due to loss of anthracene at temperatures higher than 160^{o}C.

3.8.2 Differential Scanning Calorimetry (DSC)

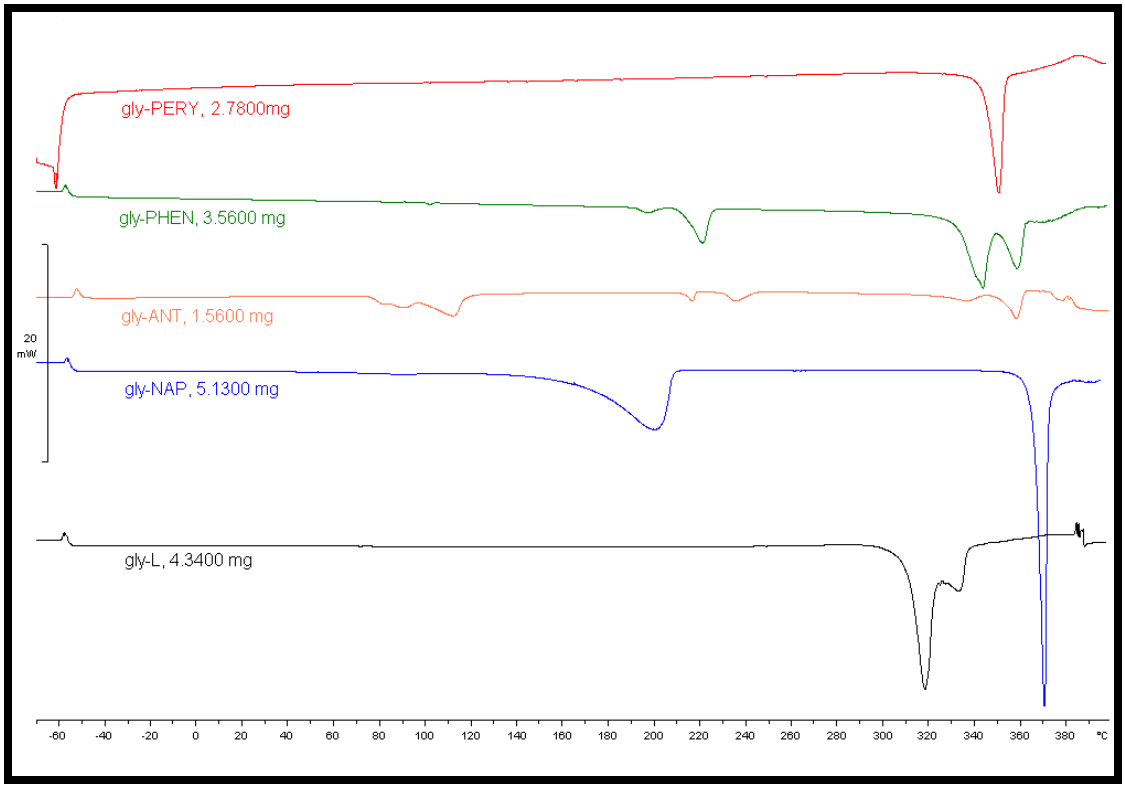

Figure 3.12: DSC curves of heat flow (mW) vs. temperature (^{o}C) for gly-L and CT complexes.

The DSC curve obtained for the gly-L and CT complexes are indicated in the figure above. The DSC scan for gly-L indicates that the material melts over a range 295-336^{o}C, and shows two endotherms with integrated values of -413.54mJ and -99.77mJ respectively. From these integral values a total enthalpy value of -38.0kJ/mol was obtained. The melting points observed from the DSC scans were significantly lower when compared to the thermal stability data obtained in the TGA. Both TGA and DSC data obtained indicates that an increase in donor size increases the thermal

stability of CT complexes. The DSC scan associated with the gly-NAP complex indicates that naphthalene escapes over a range of 142-213^{o}C, with a peak value of 147.44^{o}C and an enthalpy value of -81.7kJ/mol. The gly-ANT scan indicated the liberation of the solvent molecules at a temperature below 117^{o}C, followed by the melting of anthracene. gly-PHEN indicated a two stage melting of the phenanthrene molecules at 203.31^{o}C and 219.36^{o}C and was responsible for an enthalpy of fusion of -23.9kJ/mol. From all DSC scans gly-PERY was the only complex to contain a single peak with a melting point of 342.02^{o}C correlating to an enthalpy of -94.7kJ/mol.

3.9 Spectral Analysis

3.9.1 Solid state UV-Vis

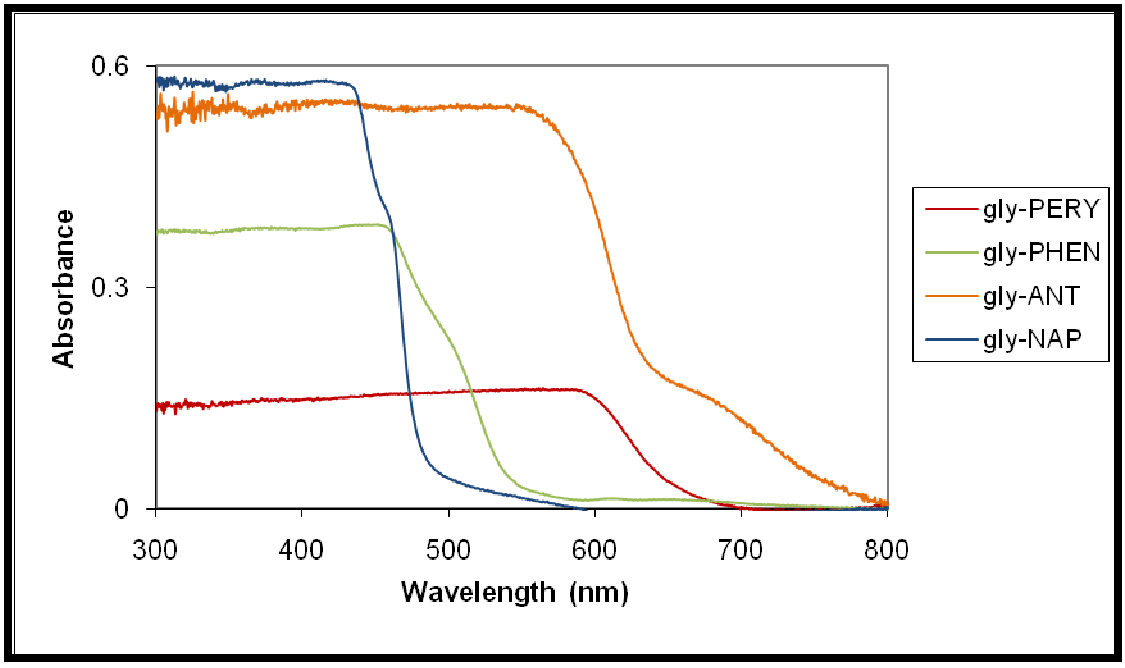

Figure 3.13: Solid state UV-Vis spectra for gly-L CT complexes reported here.

Figure 3.13 shows the UV-Vis absorption spectra in the solid state of the various CT complexes formed with gly-L. All CT complexes exhibit transition bands at different positions as is due to the difference in electronic charge being transferred from a donor to an acceptor molecule. All the complexes except for gly-PERY contain at least two transition bands. The band energies differ amongst the CT complexes, with

gly-ANT absorbing at the lowest energy band of 149kJ/mol at 800nm, followed by gly-PERY with 166kJ/mol at 721nm, gly-NAP with 200kJ/mol at 597nm and lastly gly-PHEN with 205kJ/mol (584nm).

3.9.2 Liquid state UV-Vis

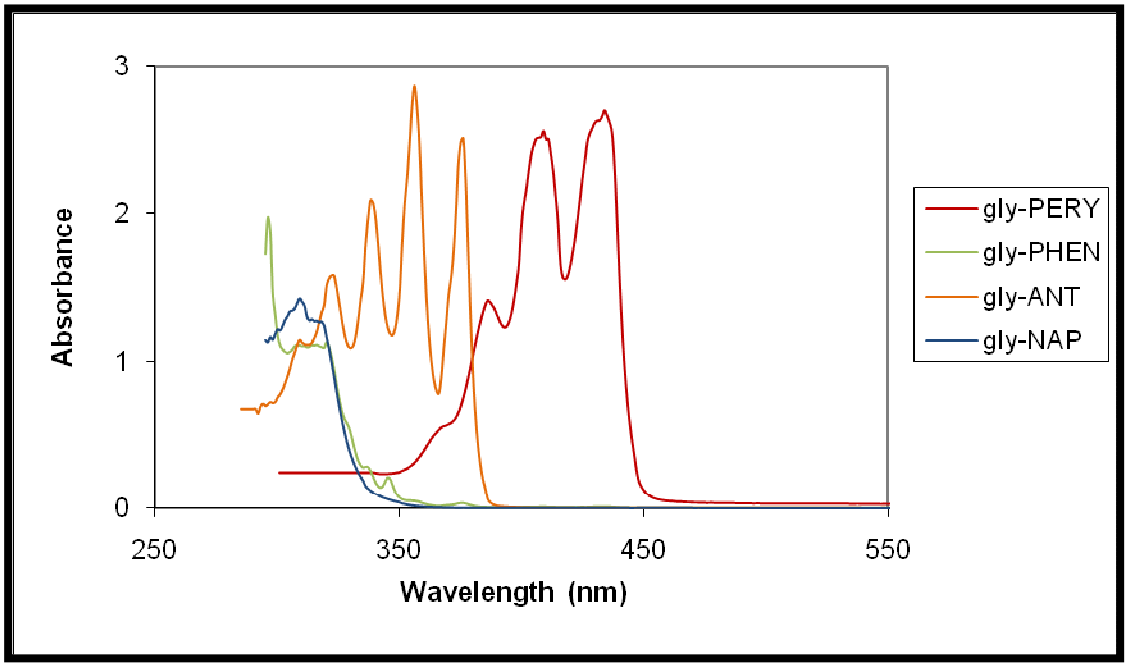

Figure 3.14: UV-Vis spectra for CT complexes formed with gly-L measured in solution.

The above UV-Vis spectra indicate the absorbance bands of the CT complexes formed with gly-L. The number of absorption bands in solution differed amongst the CT complex with gly-NAP containing two bands occurring at 300-350nm, gly-ANT having five bands at 300-380nm and both gly-PHEN and gly-PERY containing three bands between 300-340nm and 350-450nm respectively. The UV-Vis spectra obtained for the CT complexes are consistent with the results obtained by Barooah (2006).

The liquid and solid UV-Vis spectra indicate different absorption energies for each of the CT complexes. The solid state illustrates much lower absorption energies (from

800nm) when compared to the liquid state (from 460nm). The most noticeable difference between these spectra is that gly-ANT has the lowest absorption energy within the solid state whereas gly-PERY has the lowest absorption energy in the liquid state.

3.9.3 IR-Spectrum

Table 3.6: Infrared spectral data for gly-L and CT complexes.

Complexes	Ar (C−H) (donor)	Ar (C−H) (acceptor)	C=O	C-N	COOH	C−H_2
gly-L (cm^{-1})	738M	812 W	1708 M	1116M	1708M & 1244M	1392M
gly-NAP (cm^{-1})	739S	891 W	1710M	1116M	1710S &1250M	1384 - 1400M
gly-ANT (cm^{-1})	730S	889M	1702M	1184 W	170M & 1251 W	1384 - 1400M
gly-PHEN(cm^{-1})	738S	817W	1714M	1118 M	1714M & 1238M	1382- 1400M
gly-PERY(cm^{-1})	740M & 769S	815M	1714M	1122M	1714 - 1253M	1381- 1402M

The above table indicates the spectral bands assigned to gly-L and all CT complexes. The peaks obtained for each spectrum occurred within the expected ranges, as seen in the table above. All spectra appeared to be very similar and the assignments were consistent with the general structure of the host and the CT complexes. The carbonyl groups (C=O and O=C-OH) overlap each other but there is an additional peak which verifies the existence of the carboxylic acid i.e.1210-1320 cm^{-1}. gly-PERY was the only complex to contain an additional C-H aromatic donor peak, thereby indicated by the presence of two C-H donor peaks.

Table 3.7: Expected values for assigned spectral bands (www.cem.msu.edu).

Assignment	Range (cm^{-1})
Ar (C−H) (donor)	725-760 STRONG
Ar (C−H) (acceptor)	800-900 WEAK
C=O	1695-1725
C-N	1000-1250
COOH	1700-1725
	1210-1320
C−H_2	1350-1470

3.10 Further Experimentation

Once the structures CT complexes were obtained further experimentation was undertaken to try and form new CT complexes. In this pursuit mixtures of anthracene and phenanthrene, anthracene and perylene, phenanthrene and naphthalene were utilised in a 1:1 ratio with gly-L. It was found that the first reaction containing anthracene and phenanthrene with gly-L, solely led to the formation of gly-ANT, as observed by optical microscopy. This result is consistent with the lattice energy lattice energy calculation in which the gly-ANT structure (lattice energy -688.90kJ/mol) was much more stable than the gly-PHEN structure (lattice energy -563.60kJ/mol).

The above lattice calculations and UV-Vis results lead to the formation of a interesting experiment, in which two donors similar in absorption and lattice energy were both placed into a vial containing gly-L molecules. The crystallisation of anthracene and perylene as well as naphthalene and phenanthrene with the gly-L host molecule lead to the formation of both crystal morphologies, as observed by optical microscopy.

Other potential donors in the form benzene, indigo, 4-amino-biphenyl and 4-amino-nitrobenzene were also tested, but attempts to form CT complexes with these compounds were unsuccessful yielding starting material only. It is likely that larger aromatic rings systems (>5 rings) would have also have lead to the formation of CT complexes; however these molecules would be difficult to use due to solubility issues.

The glycinyl positions on the pyromellitic dianhydride were also substituted with larger or more planar molecules. These included β-alanine, γ-amino–butyric acid and 4-aminopyridine. From these three attempts only β-alanine and γ-amino–butyric acid ligand crystals were successfully grown. The β-alanine derivative was synthesised and characterised by Dr. Manoj Kuchunnoonny, whereas the γ-amino–butyric acid

was grown and is presented in this study. Unfortunately the more planar 4-aminopyridine derivative could not be recrystallised, hence no crystals of this structure could be obtained.

3.11 Discussion

Crystallisation experiments of gly-L host molecule with various aromatic molecules resulted in the formation of CT complexes. CT complexes obtained in this study all adopted the same morphology but varied in colour. This formation of colour amongst the CT complexes was due to the difference in electronic charge being transferred from a donor to an acceptor molecule. This difference in charge varies amongst donor molecules and depends on its conjugation, size and shape. Thus in trying to understand the nature of these coloured complexes, further characterisation through SCXRD, and various analytical techniques were performed.

The main technique utilised in this research project was SCXRD, which showed the various packing arrangements of the host as well as CT complexes. All CT complexes reported here crystallise in a triclinic crystal system with a *P*-1 space group except for gly-ANT which crystallise in monoclinic $P2_1/c$. The molecular structures adopted by all CT complexes showed a 1:1 donor acceptor ratio. CT complexes were formed primarily due to CT $\pi\cdots\pi$ interactions and extensive hydrogen bonding interactions through the carboxylic acid groups, thereby forming 2D stacked structures. Donor acceptor planar distances for all complexes were well within the limit of 3.6Å set out by Hunter *et al*. (1990). gly-PHEN was the only complex to contain a full molecule in the asymmetric unit due to the asymmetric shape of the phenanthrene donor molecule.

All structures adopted a $R^2_2(8)$ hydrogen bonded dimer pattern, except for gly-ANT. It was noted that the carboxylic acid groups associated with gly-ANT included methanol solvent molecules that were incorporated into the carboxylic bridges (figure 3.6). Thereby leading to a $R^4_4(12)$ hydrogen bonded ring pettern. The *trans* geometry

of the carboxylic acid indicates a decrease in the offset stacking angle as the the size of the donor increases.

With the exception of gly-ANT, all 2D sheets amongst the CT complexes align in a parallel fashion resulting in the extension of the structure into the third dimension. gly-ANT adopts a zigzag arrangement due to CH···O interactions between the adjacent sheets (figure 3.8) due to the methanol molecules. Extension into the third dimension is stabilised by various intermolecular CH···O hydrogen bonding interactions between the host-host and host-guest molecules.

Lattice energy calculations revealed that the most stable structure from all CT complexes was gly-ANT (-688.90kJ/mol), followed by gly-PERY, gly-PHEN and gly-NAP. Each structure contained a unique set of molecular arrangements, of which three were common to all CT complexes. These included CT π···π stacking, and various hydrogen bond interactions.

The PXRD patterns showed that the calculated and observed pattern were very similar for all CT complexes except for gly-ANT and gly-L. The discrepancy in the gly-ANT patterns could be due to the evaporation of methanol upon grinding. Whereas the deviation observed for gly-L could be attributed to starting material.

Both TGA and DSC scans indicated the same thermal behavior of structures, in the sense that as size of the donor increases so to does its thermal stability. gly-ANT is the only structure that was not consistent with this trend due to the addition of solvent molecules within its structure.

Both the solid UV-Vis and liquid state UV-Vis differed when compared to each other indicating the effect of the crystal environment versus the liquid environment on such spectra. The most noticeable difference amongst the two spectra is that the lowest energy within the solid state corresponds to gly-ANT whereas gly-PERY contains the

lowest energy in the liquid state. The IR spectrum for gly-L and CT complexes showed that all peaks are within the expected ranges and are consistent with the general structure of host molecule and CT complexes.

3.12 References

Barooah, N., Sarma, R. J., Batsanov, A. S., Baruah, J. B. (2006). J. Molecular Structure, 8, 608.

Barooah, N., Sarma, R. J., Baruah, J. B. (2003). Crystal Growth & Design, 3, 639.

Hunter, C. A., Sanders, J. K. M. (1990) J. Am. Chem. Soc. 112, 5525

Kishikawa, K., Tsubokura, S., Kohmoto, S., Yamamoto, M. (1999). J. Org. Chem., 64, 7568.

http://www.cem.msu.edu/~reusch/VirtualText/Spectrpy/InfraRed/infrared.htm- accessed on 28/09/2009.